2024 IEEE/SICE International Symposium on System Integration (SII)
January 8-11, 2024. Ha Long, Vietnam

Analog Magnetic Sensor-Robotic System for Steel Structure Inspection

Anh Quyen Pham, Duc La, and Hung Manh La, *IEEE Senior Member*

***Abstract*— More and more steel bridge collapse accidents occur worldwide due to broken steel structures, causing significant loss of life and property to mankind. This has spurred much research into robots that can climb steel surfaces and carry smart sensors with the desire to assist inspectors in inspecting steel defects. However, current non-destructive evaluation (NDE) sensors such as eddy-current and giant magnetoresistance (GMR) are not able to be integrated with the robotic platforms due to their large size, mass, and limited ability to interface. More importantly, these NDE sensors may fail to detect hidden and underlying cracks. Therefore, in this paper, we present a novel and compact analog magnetic sensor system to detect different types of cracks in steel. Validations are carried out on a steel test plate 600mm long, 140mm wide, and 6mm thick, and precision machined by CNCs to produce various man-made cracks including penetrating cracks, surface cracks, internal/hidden cracks, and underlying cracks. These cracks have a width varying from 0.6mm to 1.2mm with different depth levels. Combined with applying the Kalman filter to the noise reduction system, the results obtained are accurate, and the response speed is fast. The sensor is small enough and has firmware/software with an interface to make it possible to be integrated with a small drone or a climbing robot to perform an in-depth inspection of the steel bridge. A demonstration of the system can be seen in this video: `https://youtu.be/OrdpLdnF1Yk`**

I. Introduction

In recent years, there have been many serious bridge collapses, causing great loss of life and material to humanity [1]–[3]. Using bridges for a long time without regular and proper inspection and maintenance is one of the main causes of bridge collapse accidents [4], [5]. The structural destruction of steel structures usually does not take place immediately, but it will take place gradually from small cracks and then grow larger before being destroyed [6], [7]. Therefore, the use of modern technologies, especially robots with smart sensors [8]–[11], helps to check the quality of the bridge more often and helps to detect potential risks of breaking steel structures on the steel bridge as small cracks so that there are timely repair plans to avoid unfortunate accidents that may occur.

Fig.1 shows two typical robotic studies in recent research and development efforts to provide robotic systems that can climb and move on steel surfaces to perform data collection and inspection of steel defects. Some significant studies include Balaguer et al. [12], [13], Huang et al. [14], and others [15]–[23].

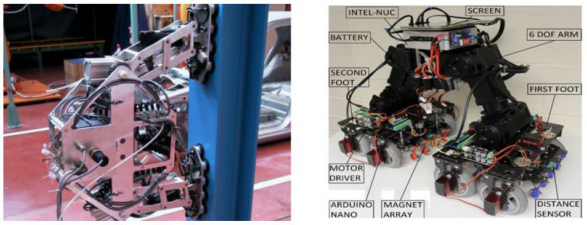

a) b)

Fig. 1: Notable robot developments for visual-based steel structure inspection, e.g., a) ROMA robot [13], and b) ARA's robot [16]

Nondestructive evaluation (NDE) methods have been used to inspect steel bridges or steel structures [24], [25]. A method of fatigue crack testing determined using fluorescence magnetic particle inspection, fluorescent penetrant inspection, and metallographic analysis, was proposed by Jeon et al. in [26]. The focused field Eddy current sensing technique was used by Xu et al. [27] to detect defects in carbon steel, and other similar works followed [28]–[33]. In other recent studies [34], [35], researchers used the Eddy current method to detect cracks in the steel. Other researchers used the Eddy current technique to measure metal thickness [36]. Notably, recent work by Otsuki et al. [37], [38] developed an ultrasonic sensor integrated with the climbing robot to measure the thickness of steel structures.

In summary, existing NDE sensors [34]–[37], [39] work well in detecting steel surface cracks and steel thickness, but often fail to detect hidden and underlying cracks due to difficulty in penetrating through.

In this paper, we present a new development of the analog magnetic sensor to detect different types of cracks in steel structures, especially detect hidden and underlying cracks where the existing sensors may not be able to [34]–[37], [39]. The central processor used is the Atmega2560 microcontroller with many supporting communication standards such as I2C and UART, which will make it easy to connect with other hardware to provide data for the process. The Kalman filter is designed and integrated to fuse raw data to improve the accuracy of the proposed sensor system. The steel sample plate measuring 600mm long, 140mm wide, and 6mm thick is precisely machined using the CNC machine to create artificial cracks ranging from 0.6mm to 1.2mm wide (typical crack sizes in steel structures [6]) at different depth levels. Transducer movement is programmed

This work was partially funded by the U.S. National Science Foundation (NSF) under grants NSF-CAREER: 1846513 and NSF-PFI-TT: 1919127, and the Vingroup Joint Stock Company and supported by Vingroup Innovation Foundation (VINIF) under project code VINIF.2020.NCUD.DA094. The views, opinions, findings, and conclusions reflected in this publication are solely those of the authors and do not represent the official policy or position of the NSF, the VINIF, or any other entities.

Anh Pham is with the AIR-VIET Corporation in Vietnam. Duc La is with the Kahlert School of Computing, University of Utah, Salt Lake City, UT 84112, USA. Hung Manh La is with the Advanced Robotics and Automation (ARA) Lab, Department of Computer Science and Engineering, University of Nevada, Reno, NV 89557, USA. Corresponding author: Hung La, email: hla@unr.edu.

2024 IEEE/SICE International Symposium on System Integration (SII) | 979-8-3503-1207-2/24/$31.00 ©2024 IEEE | DOI: 10.1109/SII58957.2024.10417657

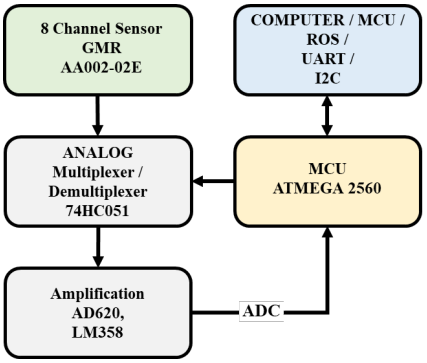

Fig. 2: Diagram of the proposed analog magnetic sensor

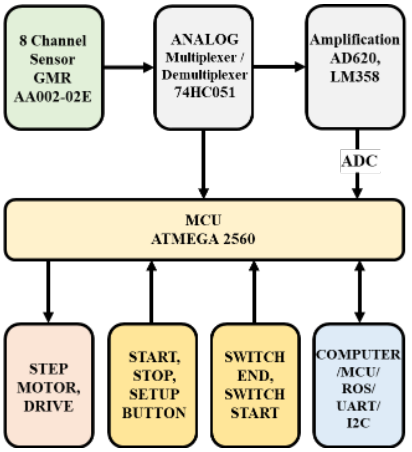

Fig. 3: Diagram of the sensor and its evaluation system to control the sensor to move along the steel plate to collect data

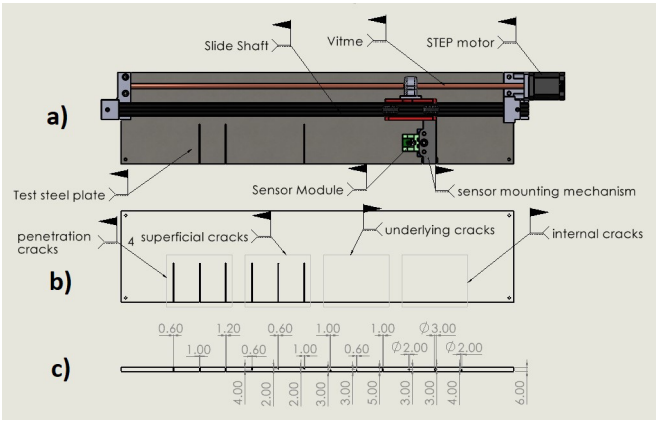

Fig. 4: Sensor evaluation system with different types of cracks: penetration, superficial, underlying, and internal

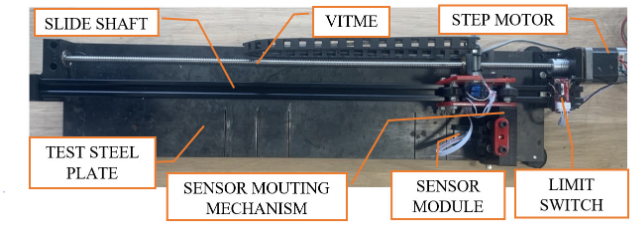

Fig. 5: Sensor evaluation system after fabrication

fully automatically to minimize possible interference factors. Difference to existing steel defect detection sensors, our developed sensor can detect cracks underneath and inside the steel plate. Comprehensive tests were performed to validate the hidden crack detection capability. The proposed sensor is then integrated into the flying-climbing robot (drone) to validate its working capability further.

II. Overall Design

The connection block diagram of the analog magnetic sensor signal processing part is shown in Fig. 2. We designed the sensor with 8 data collection channels, and each channel uses a GMR AA002-02E sensor. The data channel is selected through the channel selector using the IC 74HC4051 [40]. The signal of the selected channel then goes through the amplifier block with IC AD620 combined with IC LM358 before entering the analog-digital converter (ADC)'s reading pin of the MCU Atmega 2560. Noise is processed and filtered by the Kalman algorithm before sending the information out through the protocol UART or I2C. The Kalman filter was carefully designed and implemented in a Robotic Operating System (ROS) with optimal tuning parameters to make sure the noise was filtered out.

To ensure accurate and stable test results, we designed the mechatronic system to fully automate the test running process. The connection diagram of the whole system is shown in Fig. 3. It is similar to Fig. 2, but more functions (motor drive, buttons, and switch) are added to control the sensor to move along the steel plate to collect data.

The system's mechanical design for sensor testing is depicted in Fig. 4. Four typical types of cracks are made using the CNC machine to have the accuracy of crack size (depth and width). Type 1: *Penetrating crack* means that the crack goes through the steel plate from one side to the other. Type 2: *Hidden crack* means that the crack is inside the steel plate and can be seen from both sides of the plate. Type 3: *Superficial crack* means that the crack is on the surface of the steel plate but does not go through from one side to the other. Type 4: *Underlying crack* means that the crack is under one side of the steel plate but cannot be seen from the other side.

Fig. 5 shows the mechanical system after being fabricated/manufactured. The system consists of a NEMA17-1.8^o stepper motor, a 4mm threaded stepper screw, and a 20mm wide straight slide rail. The rail helps limit vibrations and allows the sensor probe to move precisely from position to speed. The travel distance of the sensor probe is calculated according to the number of steps of the lead screw head by the following formula:

$$B = \frac{360^o}{\alpha * \lambda * m}, \quad (1)$$

where B is the number of steps of the motor rotating per 1mm, α is the parameter of the step angle of the motor, λ is the thread pitch of the screw shaft, and m is the maximum micro-step of the stepper motor driver circuit. Each position

B obtained corresponds to the values of the analog magnetic sensor signal AA002-02 used to compare with reality on the test piece.

III. Circuit Design and Software

A. Circuit Design

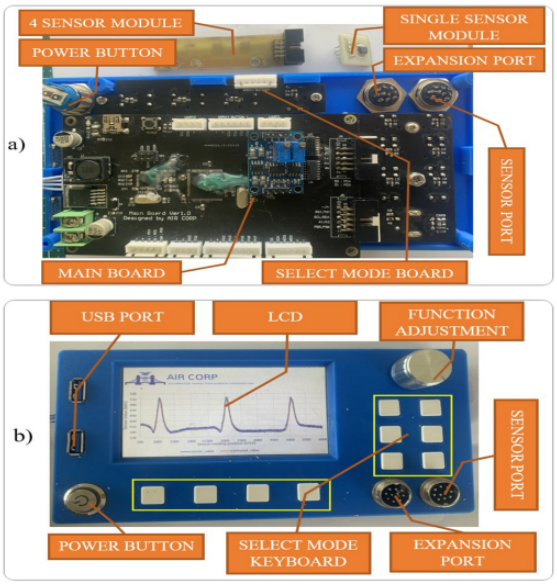

Fig. 6: a) The back of the sensor after fabrication. b) The front of the sensor with multiple buttons, ports, and LCD of 4x3 inch

We used the magnetic field sensor, AA002-02 [41] to design the probe to collect data on the steel surface. The AA002-02 has a compact size of 5.00 × 6.20 × 1.83 mm [41], which fits well with the small size of the probe and makes it suitable for integrating with small climbing robots or drones [42], [43].

The whole sensor after manufacturing is presented in Fig. 6, including the LCD of 4x3 inch to display the received sensor values directly; the buttons used for operating mode selection. A knob is used to adjust system parameters during operation, and a USB port to download the collected data. There are a sensor port and an expansion port to connect with the probe, which contacts the steel surface to collect data.

B. Kalman filter algorithm for the sensor system

The occurrence of noise that distorts the results during the measurement and data collection of the AA002-02 GMR sensor probe is difficult to avoid. In Fig.7 (blue line), the signal received from the sensor shows instability, making it difficult to identify cracks. Kalman algorithm is known as a noise filtering method, efficient prediction by observing measurements over a specified time period, which has been demonstrated in [44], [45]. The Kalman algorithm is used as a dynamical system model to predict state values, and a measurement model to correct the prediction. Due to space constraints, the detail of the Kalman filter is omitted.

The results in Fig. 7 show that the received signal is more apparent when the Kalman filter is used to remove noise.

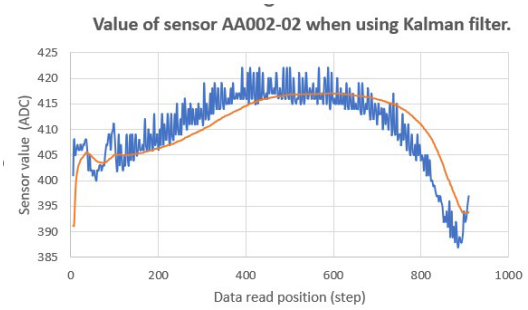

Fig. 7: Signal reading from the sensor after using Kalman filter (yellow line) vs. the raw data (blue line)

C. Software

We have developed software and firmware to allow the sensor to collect and process the data. The whole software with sudo-code integrated with Kalman filter is presented in Algorithm 1.

IV. Experimental Result

We used the sample steel plate with various types of cracks shown in Fig. 4 to conduct data measurement. We repeat the measurement 10 times and compute the average value to evaluate the crack detection ability as well as the stability of the sensor.

A. Areas with penetrating cracks

The data in Fig. 8 is the result obtained in the area of *penetration cracks*. It can be seen that the ADC value in the locations of cracks is about 100 higher than in the normal locations.

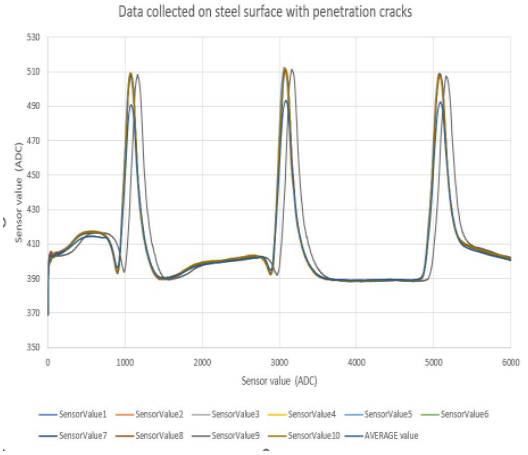

Fig. 8: Sensor data on the steel plate with *penetration cracks*

B. Areas with internal cracks

For *internal/hidden cracks*, the difference between the normal locations and the *internal crack* locations is about 10 to 40 ADC values. The results are shown in Fig. 9.

Algorithm 1: SENSOR DATA COLLECTION ALGORITHM.

Input: $(Button_{start}, Button_{reset}, Button_{stop}, Button_{up}, Button_{down})$, $(Sensor)$, $(Switch_{start}, Switch_{end})$

```
while Working mode do
    Read Button value.
    if (Button_start is pressed) then
        Active reset mode.
        Motor go to start point.
        Read travel switch value.
        while (reset mode) do
            Read travel switch value.
            if (Switch_start is pressed) then
                STOP.
                Break to reset mode.
        Active inspection mode.
        Motor go to end point.
        while (inspection mode) do
            Read travel switch value.
            Read Button value.
            Calculate current position.
            Read Sensor value.
            Apply Kalman filter for Sensor.
            Send Sensor value after applying
              Kalman filter and current position out
              via UART port.
            if (Switch_end is pressed)——(Button_stop
              is pressed) then
                STOP.
                Break to inspection mode.
            if (Button_up is pressed) then
                Increase speed by 10 unit.
            else
                if (Button_down is pressed) then
                    Decrease speed by 10 unit.
```

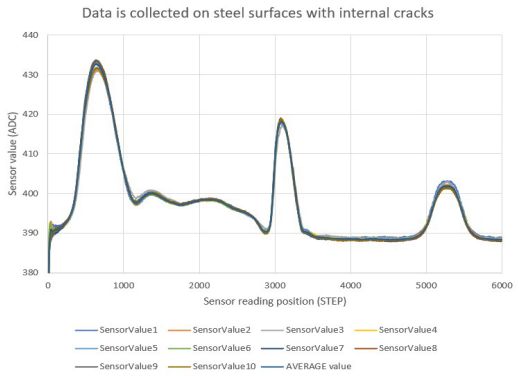

Fig. 9: Sensor data on the steel plate with *hidden cracks*

C. Areas with cracks on the surface

The results obtained in Fig. 10 are the data collected in the area of *surface cracks.* For these superficial cracks, the difference between the normal locations and the locations with superficial cracks is about 10 to 15 ADC values.

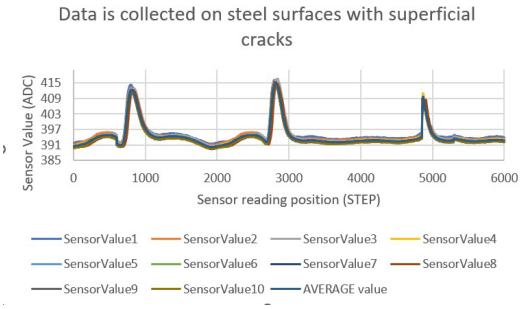

Fig. 10: Sensor data on the steel plate with *superficial cracks*

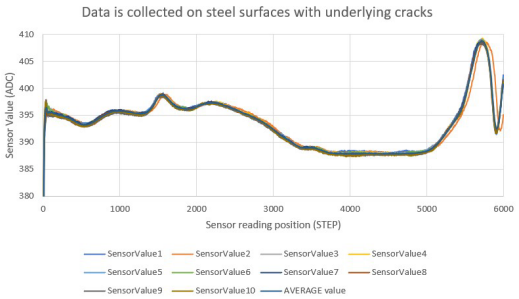

Fig. 11: Sensor data on the steel surface with *underlying cracks*

D. Areas with cracks below the surface

For the cracks underneath the steel surface, the results in Fig. 11 show that there is a difference of about 5 ADC values between the normal locations and the *underlying crack* locations, which are 1mm wide and 5mm deep. The crack locations with a width of 1mm and a depth of 3mm, and the crack locations with a width of 0.6mm and a depth of 3mm did not have notable changes in ADC values.

Through these tests (Fig. 8-11), we can see that the sensor can detect four types of cracks: *penetrating crack, internal/hidden crack, surface crack*, and *underlying crack.* For the most difficult case (the *underlying crack*), the sensor is still able to detect this type of crack with a minimum width of 1mm and a depth of 5mm. This is an important finding when compared to the existing work, which mostly is able to detect the penetrating crack and the surface crack.

E. Statistical Results

Table I shows the statistical results of the sensor. The data is collected over 20 runs on the given steel plate in Figures 4 and 5. The collected data is averaged for non-crack and crack areas. It can be seen that the sensor detects cracks well for the first three types (penetration, superficial, and internal) with different depth levels. The sensor fails to detect the *underlying crack* hidden deeper than 3 mm and the crack's width smaller than 1mm.

Type	Width (mm)	Depth (mm)	$\overline{V}_{nc}$	$\overline{V}_{c}^{max}$	Detectable
Penetrated cracks	0.6	6.0	390.1	500.3	Yes
	1.0	6.0	390.3	504.1	Yes
	1.2	6.0	389.5	508.3	Yes
Hidden cracks	2.0	3.0	390	430.2	Yes
	3.0	3.0	391	419.1	Yes
	2.0	4.0	390.5	405.6	Yes
Superficial cracks	0.6	4.0	390.4	412.4	Yes
	0.6	2.0	390.6	415.7	Yes
	1.0	2.0	389.9	409.9	Yes
Underlying cracks	1.0	3.0	390.8	393.5	No
	0.6	3.0	391.1	395.1	No
	1.0	5.0	390.5	407.8	Yes

TABLE I: Statistical results of the sensor performing an inspection on the steel plate with different types of cracks as shown in Figures 4 and 5. The average of all the values across 20 runs. $\overline{V}_{nc}$ is the average value of the sensor in the non-crack area. $\overline{V}_{c}^{max}$ is the highest average value of the sensor in the crack area.

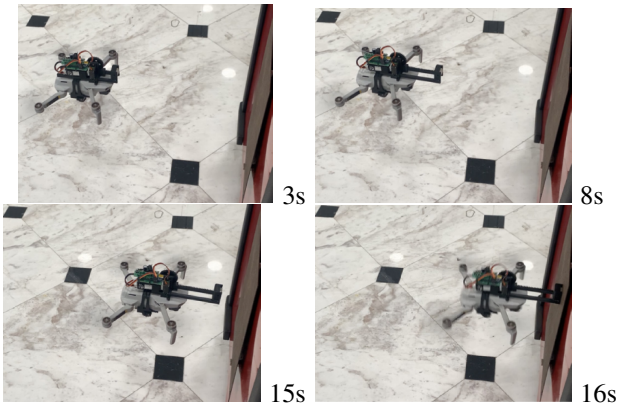

Fig. 12: Snapshots at different time stamps of a drone with a manipulator approaching the steel surface

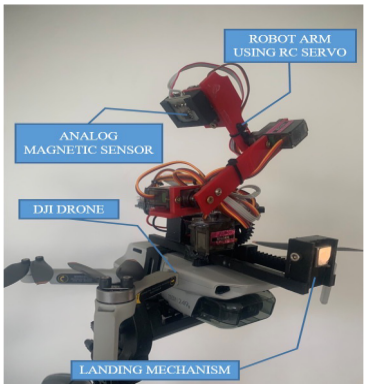

Fig. 13: Sensor integrated drone for steel structure inspection

F. Sensor-robot integration

We first designed a magnetic-based manipulator (or a landing mechanism) and integrated it with a drone. We then used our previously developed landing algorithm [17], [43] to detect available surfaces for the drone to approach. We test the drone-manipulator integration with the landing algorithm as shown in Fig.12. We can see that when the drone is close to the surface, its manipulator is gradually extended and then approaches the surface. The drone successfully adheres to the steel surface via its manipulator. When the drone firmly adheres to the steel surface, it can activate the data collection mode. When the data collection is done, the flying mode is activated, and the manipulator is released from the steel surface.

Fig. 14: Deployment of the robot on different locations for steel structure's data collection

After performing many tests to confirm the robot working/landing stably on a steel surface, we then designed and integrated a 3-DoF arm to carry the proposed analog magnetic sensor as shown in Fig. 13. This 3-DOF arm allows the drone to reach some difficult access areas like corners and joints to perform data collection and inspection. Fig. 14 shows some typical deployments of the drone with the developed sensor at multiple locations for performing inspection of steel structures.

V. Conclusion and Future Work

This work describes the new design, implementation, and testing of an analog magnetic sensor for steel structure inspection and evaluation. The results show that the sensor design works well in detecting multiple crack types (penetrating crack, internal/hidden crack, surface crack, and underlying crack). For the difficult-to-detect crack types like underlying cracks and internal cracks, the proposed sensor still shows its detection capability down to a small size of 1mm and a depth of up to 5mm. In addition to noise filtering and hardware amplification, the onboard integration of the Kalman filter was shown to be effective in filtering out the noise to obtain an accurate and smooth signal. With the results achieved, we integrated this sensor into the drone and tested it on several steel structures. In the near future, we will further modularize this sensor to have the smallest and lightest size to facilitate installation on any climbing robots [42] and drones [43], [46].

REFERENCES

[1] MNDOT, "I-35w st. anthony falls bridge collapse," *http://www.dot.state.mn.us/i35wbridge/collapse.html*, 2007.

[2] F. H. A. U.S Department of Transportation, "National bridge inventory data," *http://www.fhwa.dot.gov/bridge/nbi.cfm*, 2022.

[3] TSB, "National bridge inventory data," *http://investor.cpr.ca/news/press-release-details/2014/CP-in-full-agreement-with-TSB-incident-report-on-Bonnybrook-Bridge/default.aspx*, 2014.

[4] H. Ahmed, H. M. La, and N. Gucunski, "Review of non-destructive civil infrastructure evaluation for bridges: State-of-the-art robotic platforms, sensors and algorithms," *Sensors*, vol. 20, no. 14, 2020.

[5] N. Gucunski, H. M. La, K. Dinh, and M. Khudhair, "Advancing condition assessment of reinforced concrete bridge elements through auto., visualization, and improved interpretation of multi-nde technology data," *Materials Evaluation*, vol. 81, no. 1, pp. 56–66, 2023.

[6] W. C. Cui, "5 - fatigue cracking in aged structures," in *Condition Assessment of Aged Structures*, ser. Woodhead Publishing Series in Civil and Structural Engineering, 2008, pp. 107–148.

[7] U. H. Billah, H. M. La, and A. Tavakkoli, "Deep learning-based feature silencing for accurate concrete crack detection," *Sensors*, vol. 20, no. 16, 2020.

[8] R. S. Lim, H. M. La, and W. Sheng, "A robotic crack inspection and mapping system for bridge deck maintenance," *IEEE Trans. on Auto. Science and Engineering*, vol. 11, no. 2, pp. 367–378, 2014.

[9] S. Gibb, H. M. La, T. Le, L. Nguyen, R. Schmid, and H. Pham, "Nondestructive evaluation sensor fusion with autonomous robotic system for civil infrastructure inspection," *Journal of Field Robotics*, vol. 35, no. 6, pp. 988–1004, 2018.

[10] S. Gibb, T. Le, H. M. La, R. Schmid, and T. Berendsen, "A multi-functional inspection robot for civil infrastructure evaluation and maintenance," in *2017 IEEE/RSJ Intern. Conf. on Intelligent Robots and Systems (IROS)*, 2017, pp. 2672–2677.

[11] T. Le, S. Gibb, N. Pham, H. M. La, L. Falk, and T. Berendsen, "Autonomous robotic system using non-destructive evaluation methods for bridge deck inspection," in *2017 IEEE Intern. Conf. on Robotics and Auto. (ICRA)*, 2017, pp. 3672–3677.

[12] C. Balaguer, A. Giménez, J. M. Pastor, V. Padron, and M. Abderrahim, "A climbing autonomous robot for inspection applications in 3d complex environments," *Robotica*, vol. 18, no. 3, pp. 287–297, 2000.

[13] C. Balaguer, A. Gimenez, and C. Abderrahim, "Roma robots for inspection of steel based infrastructures," *Industrial Robot: An Inter. J.*, 2002.

[14] H. Huang, D. Li, Z. Xue, X. Chen, S. Liu, J. Leng, and Y. Wei, "Design and performance analysis of a tracked wall-climbing robot for ship inspection in shipbuilding," *Ocean Engin.*, vol. 131, pp. 224–230, 2017.

[15] S. Nguyen and H. La, "A climbing robot for steel bridge inspection," *Journal of Intelligent and Robotic Systems*, vol. 75, p. 102, 2021.

[16] S. T. Nguyen, A. Q. Pham, C. Motley, and H. M. La, "A practical climbing robot for steel bridge inspection," in *IEEE Intern. Conf. on Robotics and Auto. (ICRA)*. IEEE, 2020, pp. 9322–9328.

[17] H.-D. Bui, S. Nguyen, U. Billah, C. Le, A. Tavakkoli, and H. M. La, "Control framework for a hybrid-steel bridge inspection robot," in *IEEE/RSJ Intern. Conf. on Intelligent Robots and Systems (IROS)*. IEEE, 2020, pp. 2585–2591.

[18] A. Q. Pham, H. M. La, K. T. La, and M. T. Nguyen, "A magnetic wheeled robot for steel bridge inspection," in *Intern. Conf. on Engineering Research and Applications*. Springer, 2019, pp. 11–17.

[19] A. Q. Pham, C. Motley, S. T. Nguyen, and H. M. La, "A robust and reliable climbing robot for steel structure inspection," in *IEEE/SICE Inter. Symp. on System Integration (SII)*. IEEE, 2022, pp. 336–343.

[20] S. T. Nguyen and H. M. La, "Development of a steel bridge climbing robot," in *2019 IEEE/RSJ Intern. Conf. on Intelligent Robots and Systems (IROS)*. IEEE, 2019, pp. 1912–1917.

[21] C. Motley, S. T. Nguyen, and H. M. La, "Design of a high strength multi-steering climbing robot for steel bridge inspection," in *IEEE/SICE Inter. Symp. on System Integration (SII)*. IEEE, 2022, pp. 323–328.

[22] N. H. Pham and H. M. La, "Design and implementation of an autonomous robot for steel bridge inspection," in *54th Annual Allerton Conf. on Communication, Control, and Computing*, 2016, pp. 556–562.

[23] H. M. La, T. H. Dinh, N. H. Pham, Q. P. Ha, and A. Q. Pham, "Automated robotic monitoring and inspection of steel structures and bridges," *Robotica*, vol. 37, no. 5, p. 947–967, 2019.

[24] S. S. Khedmatgozar Dolati, N. Caluk, A. Mehrabi, and S. S. Khedmatgozar Dolati, "Non-destructive testing applications for steel bridges," *Applied Sciences*, vol. 11, no. 20, 2021.

[25] N. Ulapane, A. Alempijevic, J. Valls Miro, and T. Vidal-Calleja, "Non-destructive evaluation of ferromagnetic material thickness using pulsed eddy current sensor detector coil voltage decay rate," *NDT & E Intern.*, vol. 100, pp. 108–114, 2018.

[26] I. Jeon, H. J. Lim, P. Liu, B. Park, A. Heinze, and H. Sohn, "Fatigue crack detection in rotating steel shafts using noncontact ultrasonic modulation measurements," *Engin. Struct.*, vol. 196, p. 109293, 2019.

[27] Z. Xu, X. Wang, and Y. Deng, "Rotating focused field eddy-current sensing for arbitrary orientation defects detection in carbon steel," *Sensors*, vol. 20, no. 8, p. 2345, 2020.

[28] Z. Xu, S. Fan, and T. Song, "Parameter identification of pulsed eddy current testing equivalent circuit model and its application to defect evaluation," *Measur. & Contr.*, vol. 54, no. 5-6, pp. 1113–1121, 2021.

[29] G. Tytko, "Eddy current testing of small radius conductive cylinders with the employment of an i-core sensor," *Measurement*, vol. 186, p. 110219, 2021.

[30] X. Li, G. Tian, K. Li, H. Wang, and Q. Zhang, "Differential ect probe design and investigation for detection of rolling contact fatigue cracks with different orientations," *IEEE Sensors Journal*, vol. 22, no. 12, pp. 11 615–11 625, 2022.

[31] J. Ge, C. Yang, F. Yu, and N. Yusa, "Transformation of the rotating eddy current testing signal at the desired eddy current orientation," *NDT & E Intern.*, vol. 125, p. 102551, 2022.

[32] A. Berkache, J. Lee, D. Wang, and D.-G. Park, "Development of an eddy current test configuration for welded carbon steel pipes under the change in physical properties," *Applied Sciences*, vol. 12, no. 1, 2022.

[33] Z. Xu, H. Chen, Z. Qu, C. Zhu, and X. Wang, "Nondestructive testing of local incomplete brazing defect in stainless steel core panel using pulsed eddy current," *Materials*, vol. 15, no. 16, 2022.

[34] K. Tsukada, M. Hayashi, Y. Nakamura, K. Sakai, and T. Kiwa, "Small eddy current testing sensor probe using a tunneling magnetoresistance sensor to detect cracks in steel structures," *IEEE Trans. on Magnetics*, vol. 54, no. 11, pp. 1–5, 2018.

[35] Y. Li and L. Hong, "Research of eddy current sensors applied to displacement-based vector hydrophones," *Sensors and Actuators A: Physical*, vol. 331, p. 112968, 2021.

[36] A. Antony Jacob, S. Ravichandran, V. Upadhyay, P. Rajagopal, and K. Balasubramaniam, "Thickness estimation of marine structures using an rov-based pulsed eddy current technique," in *Advances in Non-destructive Evaluation*. Springer Singapore, 2021, pp. 133–143.

[37] Y. Otsuki, S. T. Nguyen, H. M. La, and Y. Wang, "Autonomous ultrasonic thickness measurement using a steel climbing mobile robot integrated with martlet wireless sensing," in *ASNT Research Symp.*, 2022.

[38] ——, "Autonomous ultrasonic thickness measurement of steel bridge members using a climbing bicycle robot," *J. of Engineering Mechanics*, vol. 149, no. 8, p. 04023051, 2023. [Online]. Available: https://ascelibrary.org/doi/abs/10.1061/JENMDT.EMENG-7000

[39] Olympus, "Thickness and flaw inspection solutions nortec 600," in *https://www.olympus-ims.com/en/nortec600/*, 2022.

[40] T. Instruments, "High speed cmos logic analog multiplexers/demultiplexers," *74HC4051 Datasheet*, access 2022.

[41] N. CORPORATION, "Aa/ab-series analog magnetic sensors," *AA002-02E Datasheet*, access 2022.

[42] S. T. Nguyen, H. Nguyen, S. T. Bui, V. A. Ho, T. D. Ngo, and H. M. La, "An agile bicycle-like robot for complex steel structure inspection," in *Inter. Conf. on Robotics and Auto. (ICRA)*, 2022, pp. 157–163.

[43] A. Q. Pham, A. T. La, E. Chang, and H. M. La, "Flying-climbing mobile robot for steel bridge inspection," in *IEEE Inter. Symp. on Safety, Security, and Rescue Robotics (SSRR)*, 2021, pp. 230–235.

[44] H. M. La, R. S. Lim, B. B. Basily, N. Gucunski, J. Yi, A. Maher, F. A. Romero, and H. Parvardeh, "Mechatronic systems design for an autonomous robotic system for high-efficiency bridge deck inspection and evaluation," *IEEE/ASME Trans. on Mechatronics*, vol. 18, no. 6, pp. 1655–1664, 2013.

[45] H. M. La, N. Gucunski, K. Dana, and S.-H. Kee, "Development of an autonomous bridge deck inspection robotic system," *Journal of Field Robotics*, vol. 34, no. 8, pp. 1489–1504, 2017.

[46] Y. Alghamdi, A. Munir, and H. M. La, "Architecture, classification, and applications of contemporary unmanned aerial vehicles," *IEEE Consumer Electronics Magazine*, vol. 10, no. 6, pp. 9–20, 2021.